STOP 1. Eastern Concrete Crushed Stone Quarry, 1 Railroad Ave, Glen Gardner, NJ Trip leader G.C. Herman

HARD HATS REQUIRED HERE!

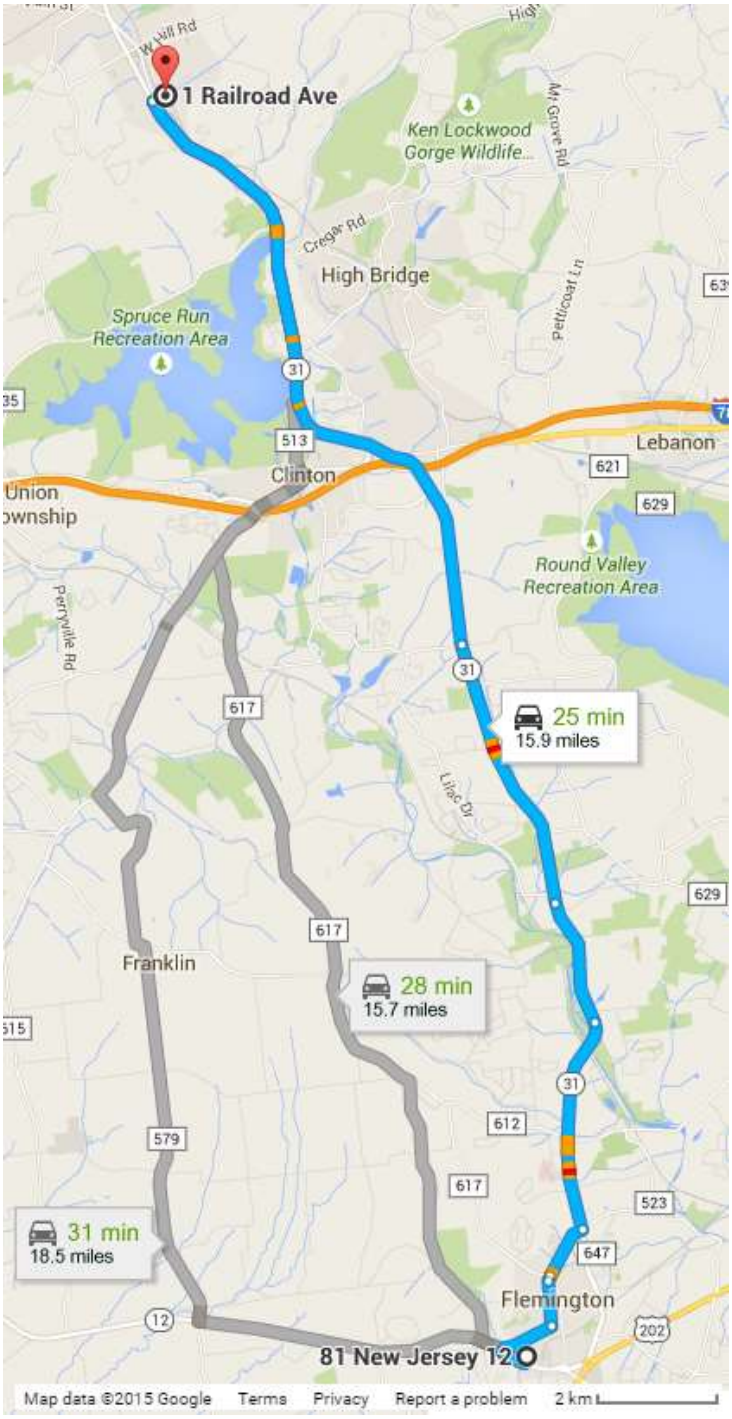

Figure 5. Google maps route (thick blue line) from the Commuter Lot at 81 NJ-12, Flemington to the Eastern Concrete quarry at 1 Railroad Ave, Glen Gardner, NJ.

Figure 5 summarizes highway routes and estimated times in driving from the meeting place to STOP 1, a crushed-stone quarry and processing plant developed on Musconetcong Mountain within crystalline basement rocks of the NJ Highlands. This quarry was targeted for study because it sits directly on a cross-strike, transtentional fault system of probable Mesozoic age that segments and offsets the mountain along its length from here to the southwest, as seen in LiDAR-based imagery (fig. 4). We see outcrop evidence of this fault system in the quarry where joints (extension fractures) and systematic, brittle, slickensided and mineralized shear planes overprint and strain earlier, ductile and brittle compressional structures stemming from earlier orogenic events. We'll examine the metamorphic compositional layering and the various ductile to brittle structures exposed in the quarry walls. The purpose of this stop is to characterize relatively late-stage, brittle strain features in the Highlands province that are also seen in the Newark Basin and demonstrate that many of the brittle, low-grade metamorphic strain mechanisms that are also seen the New Jersey Highlands and Valley

& Ridge provinces probably stem from continental rifting occurring during the Early Mesozoic period. As such, the strain effects stemming from continental breakup preceding passive-margin development are widespread, reaching past New Jersey into the Appalachian foreland of Pennsylvania (see Chapter 4). We will see evidence of copper mineralization on N-S to N20°E extension fractures, the same sets of fractures that occur in the Newark Basin and parallel deep-seated Jurassic dikes that cross-cut the Appalachian interior into the Juniata Culmination of Pennsylvania (see Chapter 4).

This quarry was mapped by the NJGWS as part of the Muessig and others (1992) field excursion focused on characterizing links between lithology and Radon occurrences in New Jersey. The geological map accompanying this report is reproduced below (fig. 6). To summarize this work with respect to our goals for this stop: the quarry is developed in Proterozoic gneisses and granites and the Longwood valley fault mapped as the contact between granitic bedrock to the southeast and gneissic bedrock to the northwest. The quartzofeldspathic gneisses contain conformable layers of amphibolite that generally strike N40°E and dip moderately to steeply southeast as well as locally disconformable alaskite lenses. Most of the rock in the quarry is sheared and shows both brittle and greenschist-grade retrograde deformation. Gross shearing appears to be sub parallel to the foliation (metamorphic layering), but small, locally localized northwest-striking brittle deformation zones are common. Most of these shear planes are coated with chlorite or epidote. Films and fibrous growths of blue crocidolite occur as an

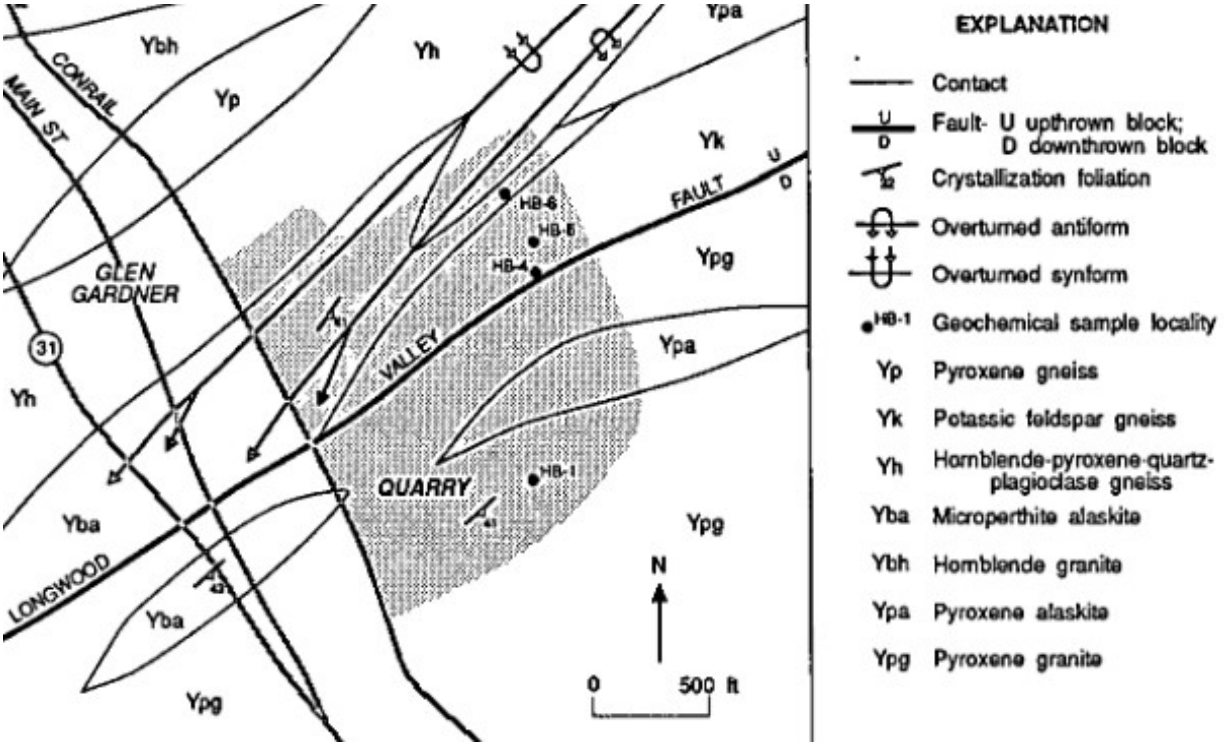

Figure 6. Geological map of the quarry in Muessig and others,

alteration product on some shear planes in the gneisses. This work also included detailed geochemical analyses of five different rock types in the quarry, documenting the link between relatively high scintillometer readings in the granites relative to the gneisses owing to increased concentrations of Uranium and Thorium. A particularly interesting part of this work is the mention and geochemical analysis of an unusual 'magnetite-rich cataclasite gneiss' that we will examine in outcrop.

I visited this quarry on a number of occasions beginning in June 2014 with various geologists from the NJGWS, Rider and Rutgers Universities in an attempt to characterize the nature of the late-stage, cross-strike faults that can be seen in LiDAR imagery (fig. 5), and that was characterized by Muessig and others (1992) as being composed of 'small' but 'common', lower-greenschist-grade, brittle shear planes. This quarry also contains two deep monitoring wells that we were given permission to log using an array of geophysical tools, including an optical borehole televiewer (BTV). Figures 7 to 15 and table 1 and 2 provide details of this recent work and a guide to the different ductile and brittle features that we will see in outcrop during this stop, including photographic details of various primary (crystalline layering) and secondary (fractures, faults, and slip lineation) structures (figs. 7, 9–12), GE maps showing some NJGWS field stations and logged wells (figs. 7 and 8), a summary of the subsurface BTV work (figs. 13 and 14), and a detailed cross-section of the hydrogeological framework based on the BTV analyses (fig. 15). Table 1 details the physical parameters for the two deep bedrock wells, and table 2 details some locations and measurement of some representative geological structures.

Outcrop data

As we enter the quarry (fig. 7), we see systematic, brittle joints, and shear planes cutting the northeast wall to our left within a well-layered quartzofeldspathic with hornblende and pyroxene. Figure 7C places these fractures into a geospatial context using an oblique southeast viewpoint and red-colored elliptical planes to show the locations and orientations of some measured metamorphic layers and superimposed shear structure detailed in table 2. The buses will park at a temporary lot located along the northern end of the eastern bench cuts near the upper quarry benches (fig. 8). We will park and assemble for a brief safety briefing and geological introduction to the quarry before walking southeast along the upper bench where the NJGWS field stations are noted in figure 8 and illustrated photographically in figure 9.

Upon starting our traverse, please be mindful that we will be examining outcrops excavated from quarrying operations. As such, before approaching any wall for close inspection, please look up above the outcrop to assess potential overhangs that look loose/perilous and avoid these locals. Please keep direct contact with the all rocks at a minimum and use rock hammers with caution as to minimize the potential for loosening any overhanging materials.

Figure 7. Photos and a map of the Glen Gardner Quarry of Eastern Concrete Materials, 1 Railroad Ave, Glen Gardner, NJ. All views are looking southeast.

A. Photo of the quarry entrance

B. Photo of the North wall just past the entrance shown above, showing a pervasive joint set in Hornblende-quartz-plagioclase gneiss that is part of the cross-strike fault system that cuts and offsets basement rocks of Musconetcong Mountain. These brittle, en-echelon, steeply dipping extension fractures show evidence of normal- and oblique-shear strain that are placed into structural and topographic context below using 3D objects (colored ellipses) in GE.

C. GE display with a monochromatic (black and white) image of the High Bridge 7-1/2' topographic quadrangle overlain atop GE imagery and set at 50% transparent. Note the two well locations (SHMW and GGQ Upper) relative to the colored ellipses represent shear fractures (red) and metamorphic compositional layering (gray). The trace of an iron (Magnetite Fe2O3)-infused, mylonite of Granville age is projected outside of the quarry along regional strike (NW-SW).

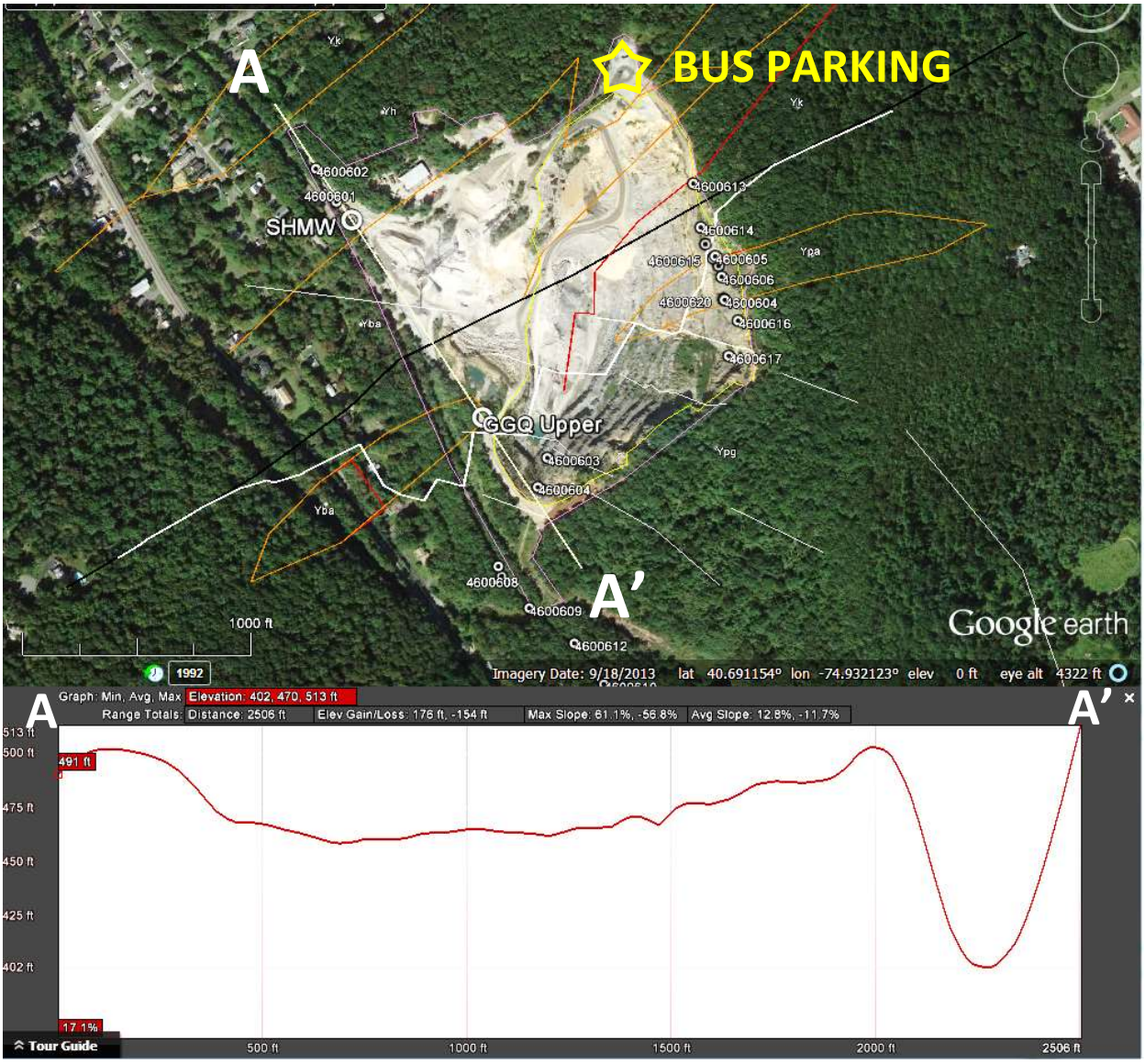

Figure 8. GE display of the quarry showing NJGWS field stations, current geological contacts (orange lines; Drake and others, 1997), a cross-section trace through two wells, and the trace of cross-strike faults that offset an older reverse fault (heavy white line). The topographic profile at the bottom was used to generate the trace of land surface for cross section A-A' (fig. 15).

Table 1. Well parameters. Geographic coordinates (WGS84 - decimal degrees), depth in feet (meters).

ID	Longitude	Latitude	Land surface (NGVD88)	Stickup	Casing depth	Total depth
SHMW	-74.933511°	40.689855°	462 (141)	2.8 (0.85)	50.0 (15.2)	
GGQ-upper	-74.933511°	40.689855°	501 (153)		25.5 (7.6)	

Table 2. NJGWS outcrop data for the Glen Garner quarry for the locations shown in figure 5-12.

Station	NJGWS-ID	Longitude	Latitude	Altitude	Dip Azimuth or Trend	Dip or Plunge	Note
GGQ1	4600601	-74.935810	40.692460	437.2	41	74	fault
GGQ1	4600601	-74.935810	40.692460	437.2	60	49	joint
GGQ1	4600601	-74.935810	40.692460	437.2	144	87	joint
GGQ1	4600601	-74.935810	40.692460	437.2	130	34	layering
GGQ1	4600601	-74.935810	40.692460	437.2	136	35	slip-lineation
GGQ2	4600602	-74.936140	40.692860	439.6	25	85	fault
GGQ2	4600602	-74.936140	40.692860	439.6	26	84	slip-lineation
GGQ3	4600603	-74.932480	40.689380	390.7	23	66	fault
GGQ4	4600604	-74.932630	40.689030	482.2	25	85	shear plane
GGQ5	4600605	-74.929830	40.691810	669.8	130	40	shear plane
GGQ5	4600605	-74.929830	40.691810	669.8	135	35	joint
GGQ5	4600605	-74.929830	40.691810	669.8	315	58	joint
GGQ5	4600605	-74.929830	40.691810	669.8	95	22	layering
GGQ6	4600606	-74.929720	40.691560	677.7	20	83	shear plane
GGQ6	4600606	-74.929720	40.691560	677.7	102	32	layering
GGQ7	4600607	-74.929670	40.691280	685.6	105	75	blue-shear-plane
GGQ8	4600608	-74.933253	40.688080	476.0	5	74	shear plane
GGQ8	4600608	-74.933253	40.688080	476.0	35	85	shear plane
GGQ8	4600608	-74.933253	40.688080	476.0	10	75	shear plane
GGQ8	4600608	-74.933253	40.688080	476.0	102	74	shear plane
GGQ8	4600608	-74.933253	40.688080	476.0	40	50	shear plane
GGQ8	4600608	-74.933253	40.688080	476.0	30	80	shear plane
GGQ8	4600608	-74.933253	40.688080	476.0	215	20	slip-lineation
GGQ9	4600609	-74.932760	40.687580	453.0	55	80	shear plane
GGQ9	4600609	-74.932760	40.687580	453.0	42	70	shear plane
GGQ11	4600611	-74.933200	40.687962	481.0	318	80	shear plane
GGQ12	4600612	-74.932050	40.687160	446.7	290	66	shear plane
GGQ12	4600612	-74.932050	40.687160	446.7	38	58	shear plane
GGQ13	4600613	-74.930170	40.692680	683.2	22	34	shear plane
GGQ14	4600614	-74.930050	40.692150	670.6	20	30	shear plane
GGQ14	4600614	-74.930050	40.692150	670.6	125	19	slip-lineation
GGQ15	4600615	-74.929860	40.691780	670.6	130	77	fault
GGQ15	4600615	-74.929860	40.691780	670.6	135	33	layering
GGQ15	4600615	-74.929860	40.691780	670.6	165	70	slip-lineation
GGQ16	4600616	-74.929460	40.691030	666.7	128	40	thrust fault
GGQ17	4600617	-74.929610	40.690610	674.6	145	70	shear plane
GGQ17	4600617	-74.929610	40.690610	674.6	105	70	shear plane
GGQ17	4600617	-74.929610	40.690610	674.6	175	29	layering

South-southwest view. The white line highlights the bench that we walk out on.

Southwest view along Musconetcong Mountain from midway along the upper bench noted above

Northeast view of the southeast bench cuts with the southeastern contact of the iron-impregnated shear zone traced with a white line. The numbered points indicate where photos were taken.

Figure 9. Photographs of the quarry. ECM mining engineer Michael Guida looks on.

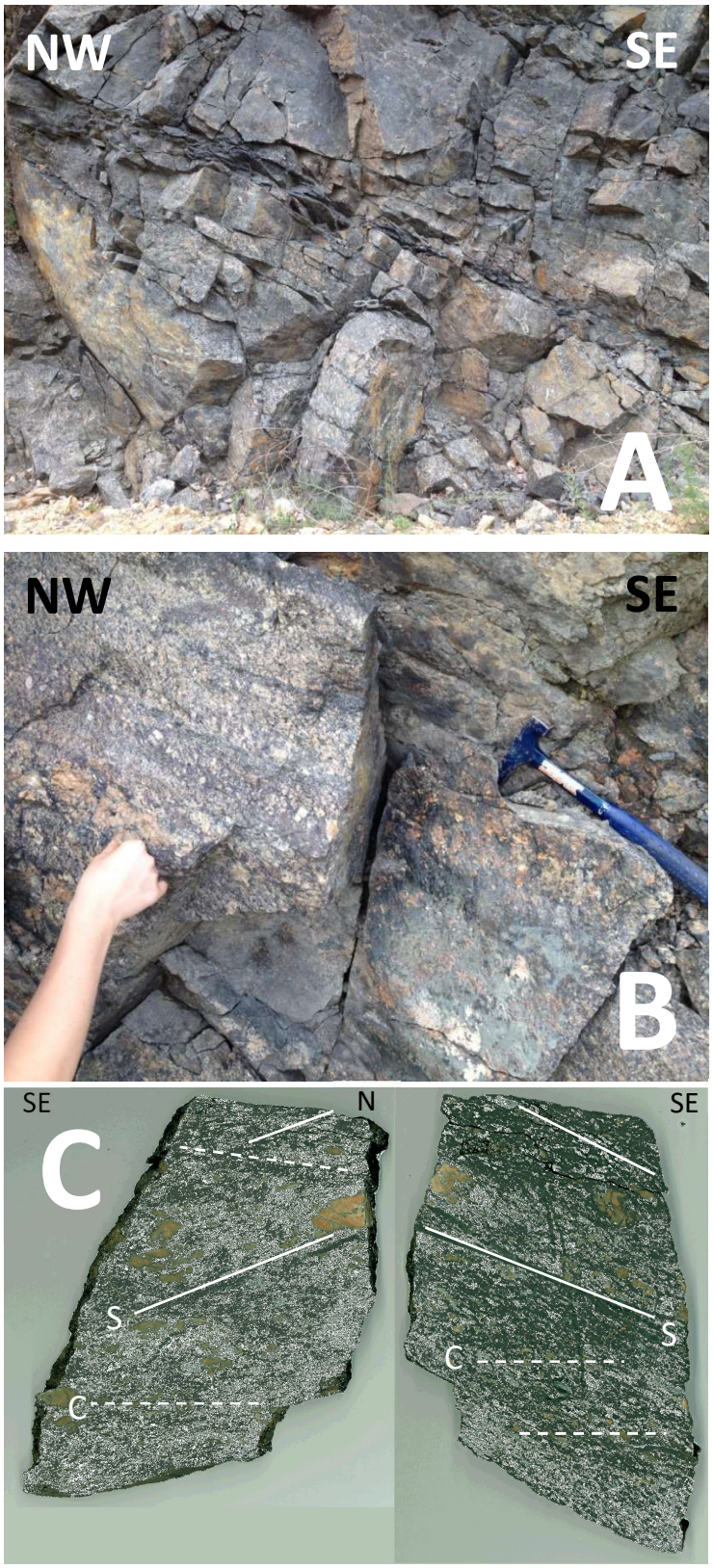

Figure 10. Outcrops near point 2 on fig. 8 showing a gently dipping brittle reverse fault (probable Alleghanian-aged) with reactivated normal slip dipping southeast and sub-parallel to a thick, Grenville-age, iron-rich (magnetite) ductile-brittle shear zone (tectonite).
A. A brittle reverse fault of probable Alleghanian age places dark grayish green pyroxene granite in the hanging wall over a very thick iron-rich tectonite occupying the footwall.
B. A close up of the old tectonite showing compositional layering with large phenocrysts and porphyroclasts including K-spar (pinkish-orange). This footwall sequence is about 20 meters thick and composed of about 20-30% magnetite in places, some of which forms in pressure shadows around siliceous porphyroclasts. This material probably formed deep within the crust (~>12 km) by synchronous magmatic intrusion and shearing between a large, granitic intrusion and older gneiss. Note the cross-cutting, brittle, slickensided shear plane to the left of the letter **B** with slickenlines pitching steeply to the southeast.
C. Photographs of a slabbed section of the iron-rich tectonite with white graphics emphasizing the SC-mylonite fabric. The area with magnetite is accentuated by adjusting image palette colors for pixels corresponding to magnetite from dark gray to light gray to contrast with the dark green and pink (K-spar) siliceous material.

Relatively fresh bedrock begins in the wall cuts near the red line drawn on figure 8, about one-third of our way to the southeast from where the buses are parked to the southeastern corner of the quarry. Before this, on your left, you can see bench cuts in sedimentary colluvium atop bedrock residuum and regolith as you proceed towards point 1 in figure 9. Here we see well-layered gneiss dipping moderately southeast before crossing the Longwood fault into the more granitic material at stations 2 to 4 (fig. 9). As illustrated above in figure 9C, the contact between the gneiss and granite is the old, magnetite-infused shear zone of Muessig and others (1992). The mining engineer excludes this from aggregate-resource use owing to its anomalously high iron content and specific gravity (density). Muessig and others (1992) geochemical analysis of this material shows Fe_2O_3 levels at about 23%, without providing photographs or further description of the material, other than designating it as a "Magnetite-rich cataclasite." As shown in figure 11, this cataclasite is a thick tectonite having a SC-planar fabric arising from heterogeneous layering and alignment of feldspar-dominated porphyroclasts (S-plane) and a second set of less-pronounced, but penetrative, mineralized (C) planes aligned acutely to layering.

At least two, brittle-deformation phases cross cut this old, ductile-brittle fabric (figs. 10A and B). SC cataclasite can form at mid-crustal depths of 5-10 km as a result of synchronous shearing, brecciating, and recrystallization (Lin, 1999), but these rocks are feldspar dominated and could have formed at deeper crustal levels (Fossen, 2010). Muessig and others (1992) report geochemical dissimilarities in some trace-element concentrations for the respective pyroxene granites, alaskite, and cataclasite, but only a few geochemical analyses were reported for representative samples of each metamorphic body, and it's probably more than coincidental that this iron deposit lies at the contact between the large igneous body of pyroxene alaskite and granite continuing southeast of the shear zone in contrast with the large body of country gneiss in the footwall to the northwest; that is, it's likely that the iron-impregnated shear zone formed during synchronous emplacement of the granite and deep crustal shearing occurring deep within the roots of the Grenville Orogen. The immiscibility of iron and silica within crustal melts is well known (Phillpotts, 1979), and this deposit either represents deep crustal fractionation of immiscible liquids during granitic emplacement into gneissic crust with synchronous shearing, crystallization and brecciation, or as Rich Volkert suggests,[1] it may be a mid- to upper crustal brittle fault of Grenville age that developed within a precursor, iron-laden metamorphic layer. The nature of this unusual iron deposit could benefit from a more thorough petrologic investigation, and serve as a key for understanding the petrogenesis of other magnetite deposits in the Reading Prong.

[1] Personal communication July 6th, 2015

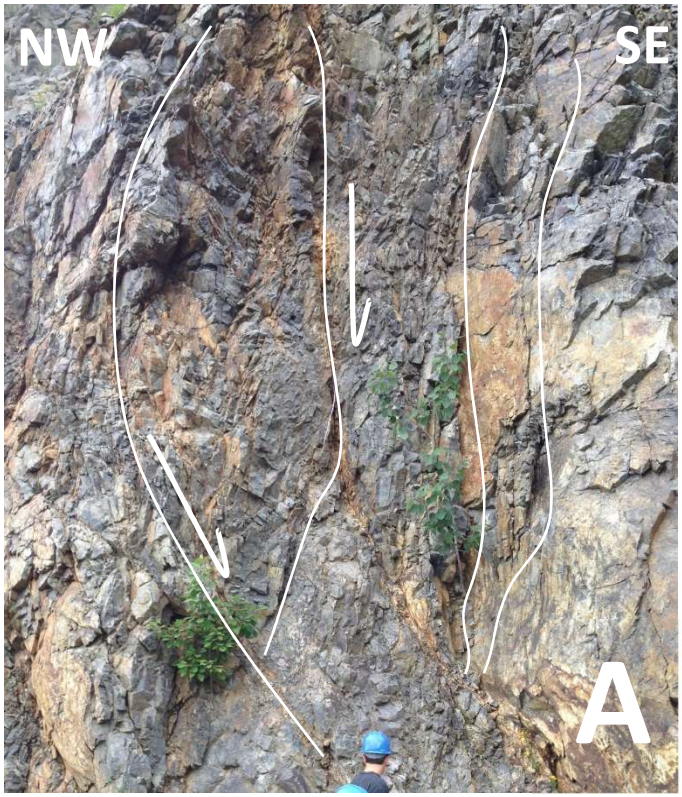

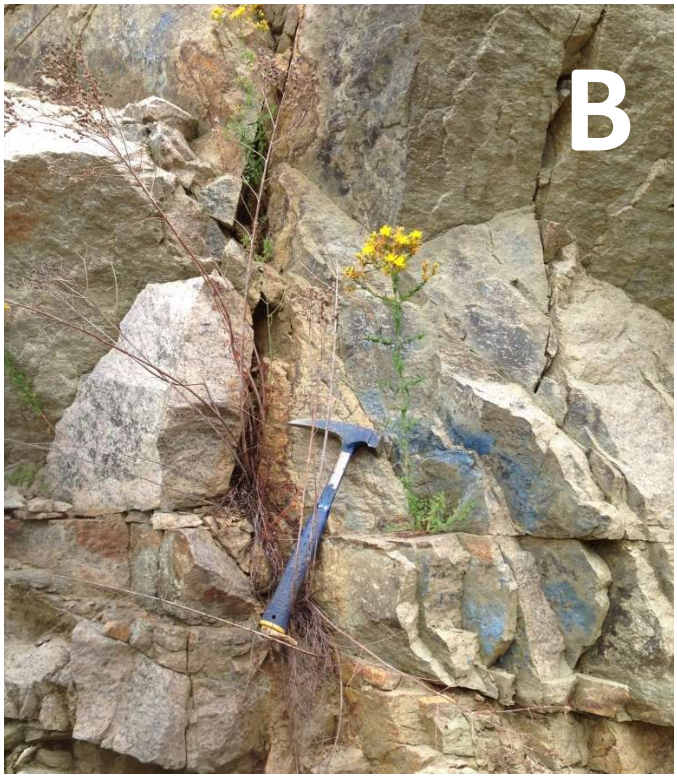

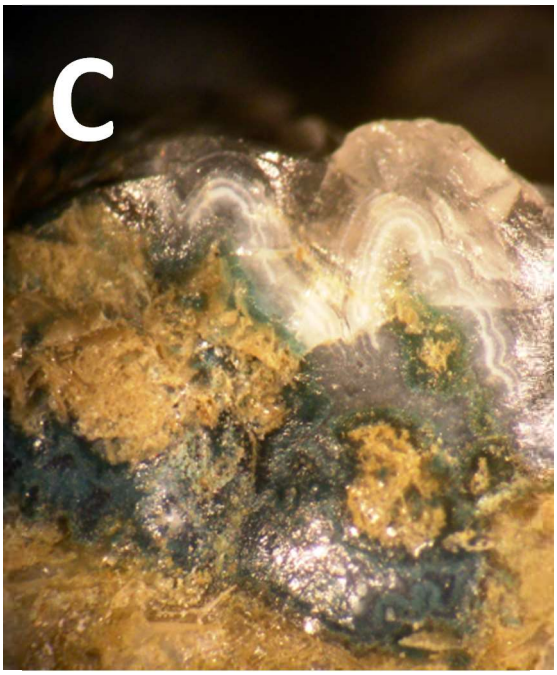

Figure 11. Photos taken near points 3 and 4 on figure 9.

A. Steeply dipping normal faults of probable Mesozoic age have branching and anastomosing fault geometry with fault blocks bounded by slickensided shear planes.

B. Electric-blue chrysocolla, a hydrated copper cyclosilicate mineral ($((Cu,Al)_2H_2Si_2O_5(OH)_4 \cdot nH_2O)$) occurs on steeply dipping extension fractures striking north to northeast, the same joint sets commonly mapped in the Newark Basin (Herman, 2009).

C. Photomicrograph at about 20X of botryoidal microcrystalline silica atop greenish chrysocolla with an unidentified rusty mineral.

Other, gently dipping, ductile-brittle, shear zones having SC fabric occur further along in these cuts (fig. 12A) that strike sub parallel to the SC cataclasite. These older shear zones are

Figure 12. Outcrops along the upper bench near point 3 (fig. 9) on the Northeast cut face.

A. Probable Grenville-age (Precambrian) ductile-brittle shear zones cutting pyroxene alaskite. These shear zones also have anastomosing (SC- tectonite) fabric and, iron-rich (chloritic) shear planes showing top-to-the-left (northwestern-directed) synthetic shearing.

B. Brittle shear zone of probable Alleghanian (late Paleozoic) age reverse (thrust) fault with reactivated, probable Mesozoic, dip-slip to the southeast. Mike Castilli of the NJGWS provides a scale.

then cut by younger, southeast-dipping, brittle reverse faults (fig. 10A and 12B) of probable Paleozoic age. Lastly, the brittle reverse faults that we see here are both reactivated with normal slip and interact with steeply-dipping normal and oblique-slip shear planes that together (figs. 10B and 12) comprise a cross-strike transtentional fault system as portrayed in figures 5 and 7C, and further described in a regional perspective in Chapter 4. As we will see in the BTV-based cross section below, this type of penetrative, brittle fracturing and shearing occurs on penetrative sets fault blocks that take on a rhombohedral-form through the interaction of faults and extension fractures of both synthetic (SE) and antithetic (NW) dips. A schematic portrayal of the angular shear and shear sense that metamorphic layering sustains from these distributed strains, at the scale of the outcrop, are characterized below using the

structural results of the two BTV surveys in the quarry wells used to monitor the water table (fig. 8 and Table 1) allows the crust to stretch and sag during continental rifting.

Borehole Televiewer (BTV) study

ECM mining engineer Michael Guida arranged for the NJGWS to log ECM's monitoring wells using our suite of slim-line geophysical equipment in order to assess the framework of this fractured-bedrock aquifer. Michael Gagliano and Michelle Kuhn of the NJGWS collected borehole and fluid electrical, caliper (borehole diameter), natural gamma radiation, and optical borehole imaging logs on June 24, 2014. The well location and construction parameters are listed in table 1. Each record was interpreted by measuring primary metamorphic layering and secondary brittle structures in each borehole image to determine the types and relative densities of the most commonly fracture and fault planes (figs. 13-15). The BTV imagery and structural results were then used to characterize some stratigraphic and structural details of the hydrogeological framework.

Many details surrounding the logging, interpretation, and structural methods used to characterize this fracture-bedrock aquifer surpass the scope of this field report, and additional structural analyses remain to be done on these records. For example, the structural classification and analyses included here stem from an initial interpretation of these records that combines the structural analyses of both wells for the purpose of constructing a representative, a schematic cross-section interpretation (figs. 13-15). Further discrimination between primary and secondary structures in each well and for the different rock type (gneiss and granite) waits, but some interesting geological relationships can be gained from the details shown here. For example, what appears to be good stratigraphic control across the distance of the quarry using a key bed (fig. 13) cannot be simply interpolated between wells based on using a n average mean orientation of metamorphic layering; that is, if one assumes that the marker horizon is the same stratigraphic layer, then there appears to be a significant amount of stratigraphic offset between the wells.

Also, the primary, reverse shear zones are oriented parallel to layering whereas the most frequently occurring shear plane is a normal, synthetic (southeast-dipping) shear plane (fig. 14) Normal reactivated slip seen on the primary, synthetic reverse work appear to have worked together to form a rhombohedral fault pattern like that commonly seen within fault zones in the Newark Basin. The apparent stratigraphic mismatch between the two wells may simply stem from an incorrect identification of two different beds as the same one. However, if the marker bed is indeed the same one, then this implies that the southeastern section here has been structurally elevated with respect to the footwall section which could arise from having intervening, unidentified reverse fault running through this quarry in the footwall of the Longwood fault. As previously mapped (fig. 6), we should have encountered the Longwood Valley and high-iron section in the wells, but we didn't. Our alternative interpretation of the

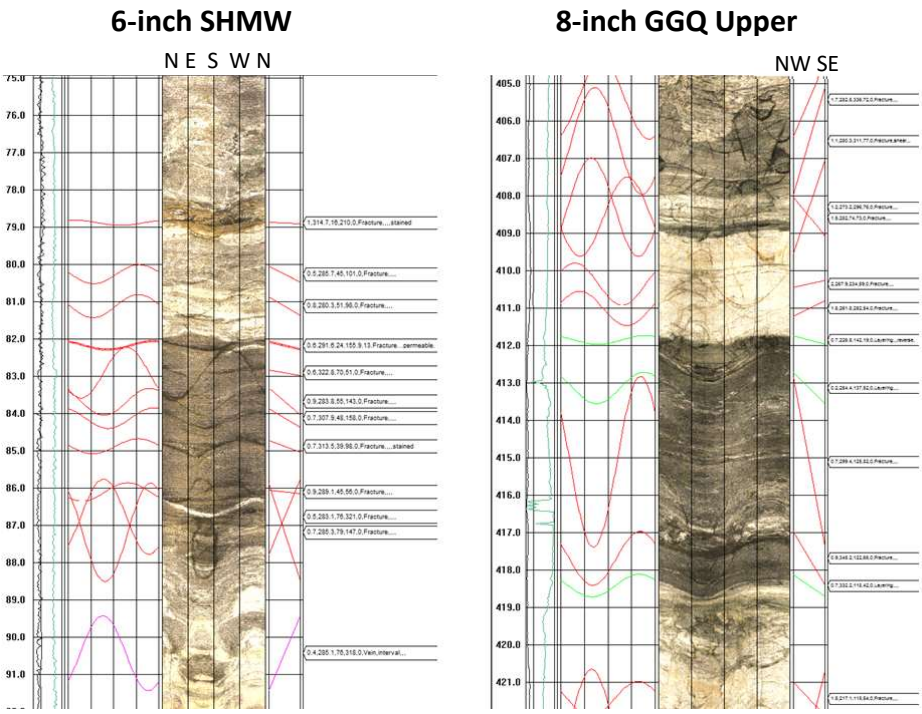

Figure 13. BTV sections from two bedrock wells in the quarry that provide stratigraphic correlation of a metamorphic contact between gneiss (NW) and granite (alaskite SE) for a distance of about 1,040 feet across strike. Well locations are mapped on figure 8.

A. Detailed sections showing unwrapped (flattened) BTV optical records next to their structural interpretations, appearing as sinusoidal line traces of fractures (red), layers (green), and shear-planes (purple).

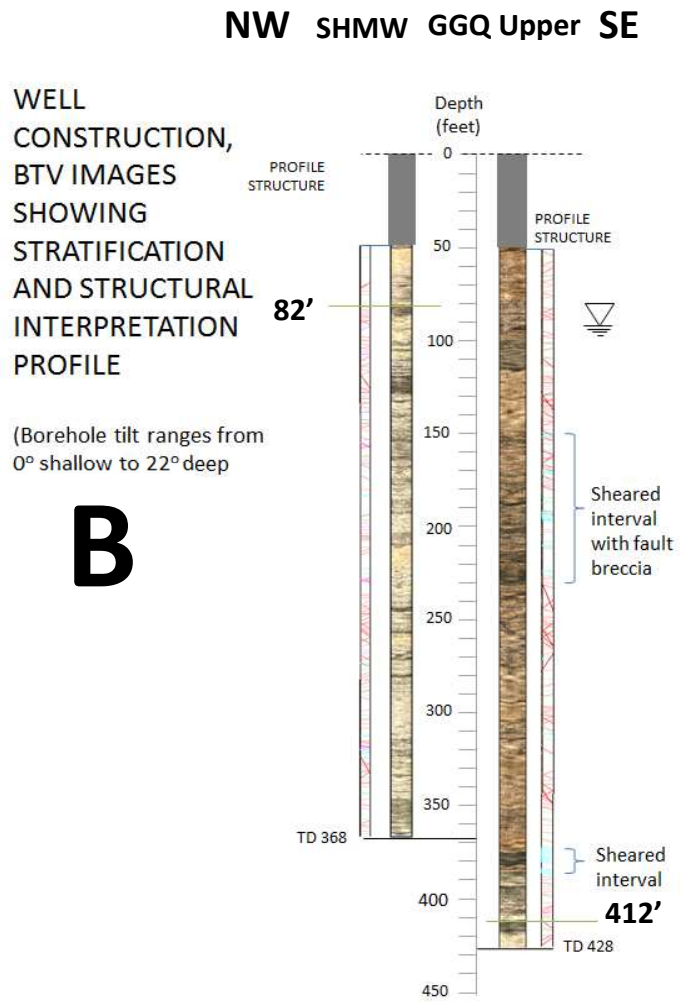

The directions noted above the SHWM BTV record are the same as for the structural interpretation to its left, and for each record. A profile depiction oriented NW-SE is shown to the right of each BTV image. The contact highlighted with the thick black arrow is a marker horizon where a thick amphibolite (darker) layer is sandwiched between quartzofeldspathic gneiss (lighter). Note the many layer-parallel brittle fractures

B. Complete optical BTV records and profile structures reproduced and placed into depth perspective relative to land surface to emphasize the color contrast between footwall gneiss on the left and hanging wall granite to the right (SE). Subsurface fault zones are also noted for the GGQ Upper well.

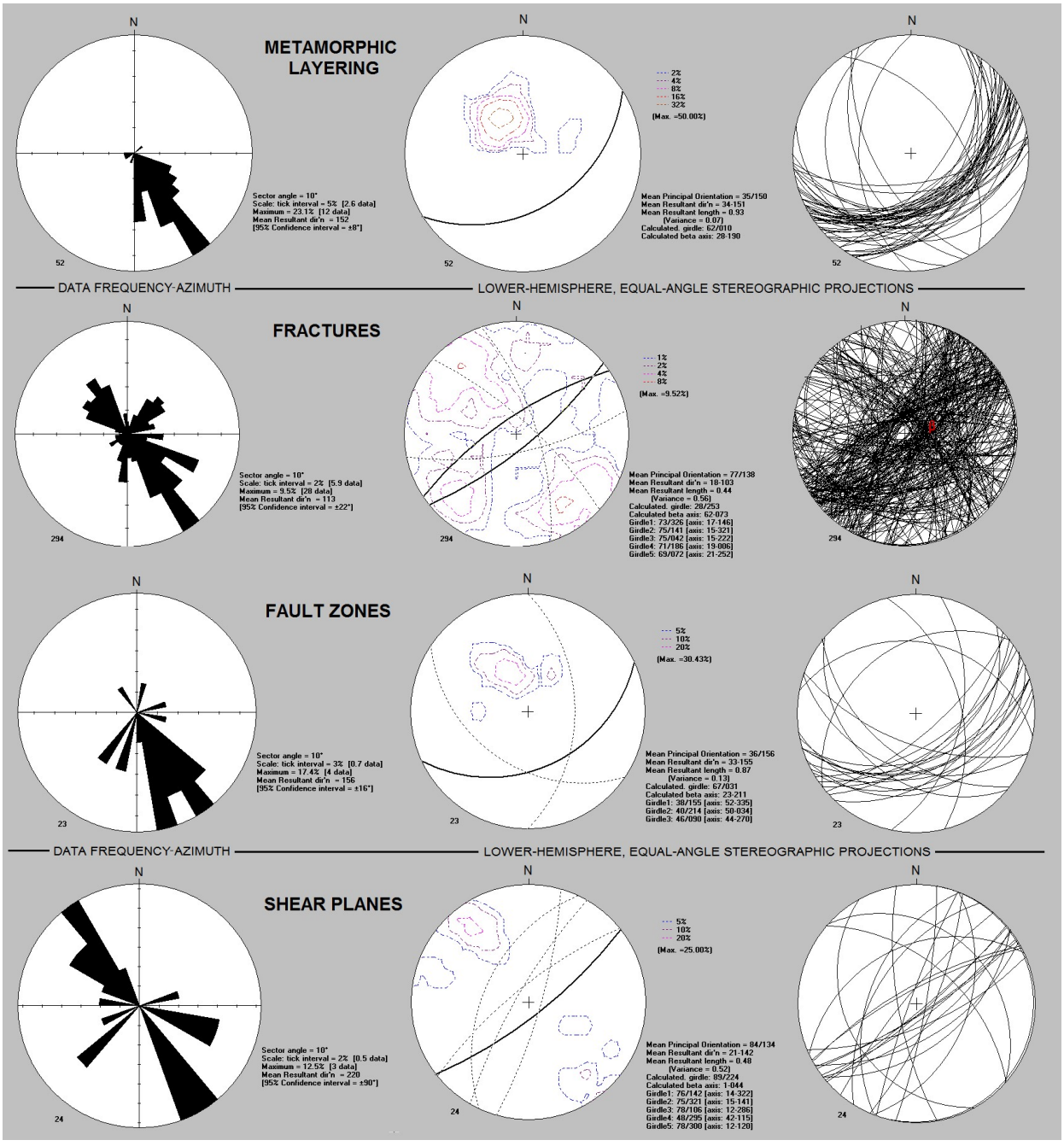

Layering	Shear fractures	Fault zones
35/150 (20%)	76/142 (20%)	38/155 (20%)
	75/321 (10%)	40/214 (10%)

Figure 14. Stereonet analyses of primary (crystalline compositional layering in metamorphic rocks) and secondary fractures, shear planes, and fault zones. Representative structural maximums with the highest percentage of occurrence are used for depicting a schematic cross-section framework of the fractured-bedrock aquifer in figure 15.

Longwood Fault, as shown in figure 8, explains why this happened. The older (1:00000-scale) version of this area didn't take into account the topographic effects on a moderately southeast-dipping fault with respect to the manner in which it deviates from a straight line on the map in coming into and leaving the quarry excavations. The actual fault trace ends up bowing considerably southeast of that previously portrayed and likely crops out in deep levels in the quarry immediately southeast of the GGQ Upper well (fig. 8).

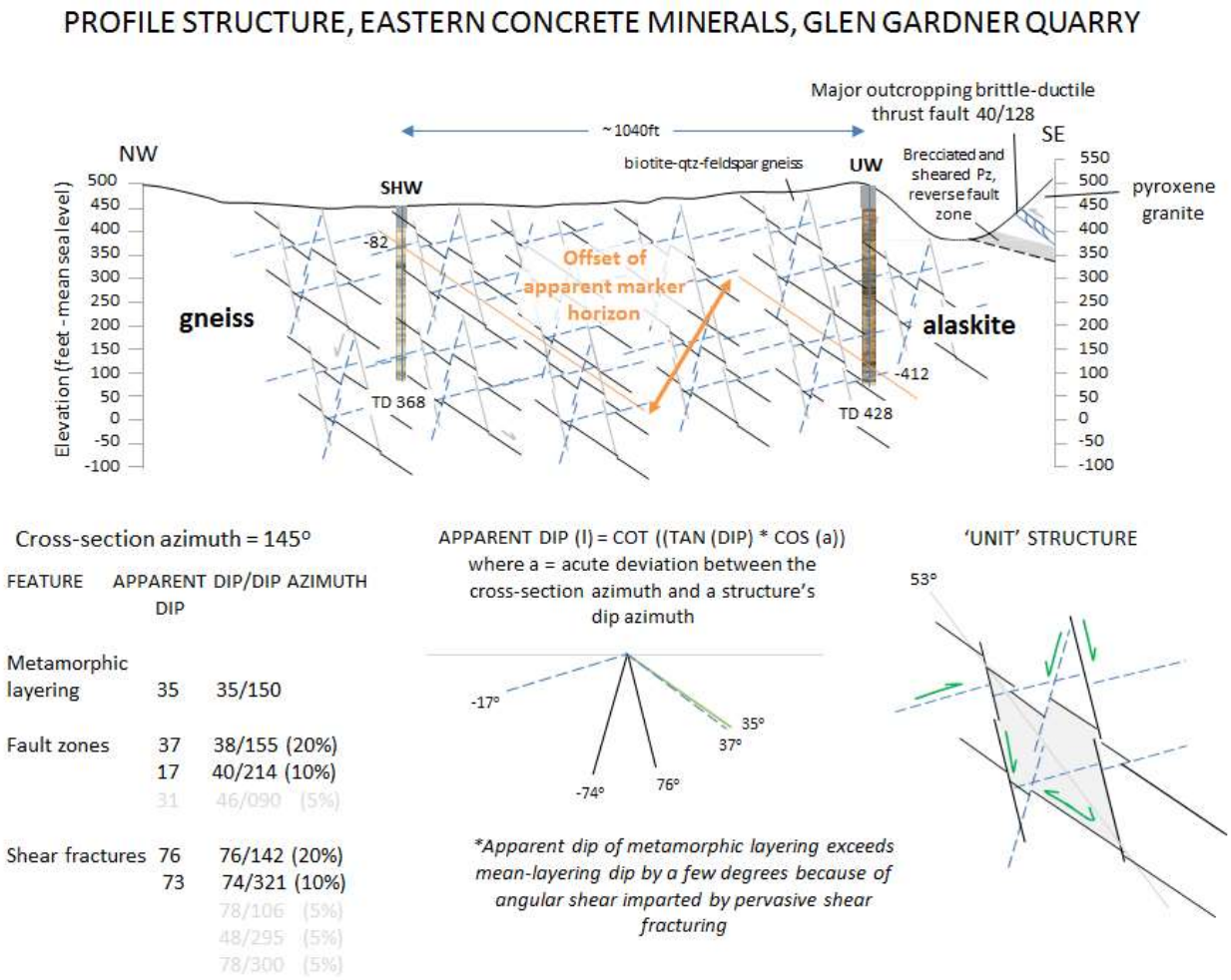

Figure 15. Schematic cross section of the Eastern Concrete quarry showing apparent dips of metamorphic layering with respect to the four principal fault planes measured in the OBI records of the quarry wells. Note the major reverse faults mapped along the SE edge of the site, and the apparent structural offset of a key bed identified in figure 13.